Eur Biophys J (1993) 22:185–194

European Biophysics Journal

The influence of the effectors of yeast pyruvate decarboxylase (PDC) on the conformation of the dimers and tetramers and their pH-dependent equilibrium

Stephan König [1], Dmitri Svergun [2,*], Michel H. J. Koch [2], G. Hübner [1], A. Schellenberger [1]

[1] Institute of Biochemistry, Department of Enzymology, Martin-Luther-University Halle Wittenberg, Weinbergweg 16a, D-06120 Halle, Germany
[2] European Molecular Biology Laboratory, Hamburg Outstation, EMBL c/o DESY, Notkestrasse 85, D-22603 Hamburg, Germany

Received: 30 March 1993 / Accepted in revised form: 24 May 1993

Abstract. The influence of effectors of yeast pyruvate decarboxylase, phosphate, pyruvamide, thiamin diphosphate and Mg^{++}, on the pH-dependent equilibrium between dimers and tetramers was studied by synchrotron radiation X-ray solution scattering. Thiamin diphosphate and phosphate shift the equilibrium to higher pH values without altering the structure of the oligomers. Pyruvamide, a substrate analogue activator, induces a significant change in the structure of the tetramer. By eliminating radiation damage by addition of dithioerythrol to the buffers, the scattering curves could be measured accurately over a large angular range. They were expanded in terms of spherical harmonics to obtain the shapes of the dimers and tetramers with higher resolution than was hitherto possible. This also allowed us to position the dimers, which are centrosymmetric at low resolution, in the tetramers which have 222 symmetry. The results indicate that addition of pyruvamide results in a less compact tetramer owing to structural changes in the dimers and to their displacements.

Key words: Allostery – Molecular model – Synchrotron radiation – Solution scattering – Spherical harmonics

Introduction

Solutions of yeast pyruvate decarboxylase (PDC), an enzyme involved in one of the steps of alcoholic fermentation, are characterized by a pH-dependent equilibrium between dimers and tetramers of the α and β subunits and the catalytic activity of the enzyme is related to the fraction of tetramers in the solutions (König et al. 1992 and references therein). In the experiments reported below, the influence of various effectors, phosphate, thiamin diphosphate and Mg^{++}, and pyruvamide, on this equilibrium was studied. Phosphate is known to enhance cooperativity in the tetramer while reducing its affinity for the substrate (Boiteux and Hess 1970). Thiamin diphosphate and Mg^{++} are the natural cofactors of PDC and their catalytic effects have been studied in detail (Schellenberger et al. 1991; Gish et al. 1988; Zeng et al. 1991). Pyruvamide can replace the substrate, pyruvate, as an activator (Hübner and Schellenberger 1986; Hübner et al. 1978) converting the reaction rate curves from sigmoid to hyperbolic. In previous experiments, radiation damage resulted in the progressive formation of octamers, an effect which made it difficult to obtain X-ray scattering patterns with good statistics. This difficulty was eliminated by addition of dithioerythrol to the buffers and more reliable scattering curves covering a larger range of scattering vectors were recorded. From these, shapes with higher resolution than those previously reported (König et al. 1992) could be obtained for the dimers and the tetramers by expansion in spherical harmonics. These allow one to place the models of the dimer in those of the tetramers and to visualize the structural change induced by pyruvamide.

Materials and methods

Preparation and assay of PDC

PDC was isolated from brewer's yeast which was broken in the vessel of a 4 l ball grinder (Maschinenfabrik Heidenau, Nagema) containing about 5 kg of glass beads with a diameter of 0.8–1.2 mm and operated at a flow rate of 3–4 l/h. About 10 kg of spin-dry yeast were suspended in 0.1 M Na-phosphate pH 6.7, 1 mM EDTA, 1 mM dithioerythrol (DTE), 5% (v/v) glycerol and 10 mg chymostatin were added immediately before breaking. Stored in separate batches at −25 °C this lysate can be kept without significant loss of activity over a period of six months. About 500 g lysate were used to prepare PDC following the methods of Sieber et al. (1983). The purified enzyme had a minimum activity of 50 U/mg (1 U corre-

* On leave from the Institute of Crystallography, Russian Academy of Sciences, 117333 Moscow, Leninsky pr. 59, Russia
Correspondence to: M. H. J Koch

sponds to 1 μmol NADH turnover/min at 30 °C) and was stored until use in 3 M ammonium sulfate at −25 °C. Immediately prior to the X-ray measurements the enzyme was recovered by centrifugation from these solutions and the pellet resuspended in a minimum volume of the buffers used for the X-ray measurements. The protein was then desalted and simultaneously concentrated (2.5–10 mg/ml) using a column (15 × 50; PD10 Pharmacia Biosystems) equilibrated and eluted with the same buffer.

In the range of pH used, from 5.5 to 9.5, all inactivation processes of the enzyme are reversible. The following buffers (Serva) were used: MES (2[N-Morpholino]-ethanesulfonic acid) from pH 5.5 to pH 6.5; HEPES (N-[2-Hydroxyethyl]piperazine-N′-(2-ethanesulfonic acid) from pH 6.5 to 8.0 and TRICIN (N-tris[Hydroxymethyl]-methylglycine) from pH 8.0 to 9.5. All buffers had an ionic strength of 0.1 and 1 mM DTE was added as antioxidant. After the change of buffer by gel filtration the effectors were added in the following concentrations in order to obtain the previously observed kinetic effects: the enzyme activator pyruvamide 250 mM; the non-competitive inhibitor phosphate 100 mM; the cofactors thiamin diphosphate (TDP) and Mg^{++} 10 mM. Enzymatic activities were measured at 340 nm and 30 °C on a DU70 (Beckman) spectrometer using the NADH/ADH system (Holzer et al. 1956). The enzyme concentrations were determined from the UV spectra by measuring the absorption difference interpolated between 240 and 340 nm at 280 nm ($\varepsilon = 281\,000\ M^{-1}\,cm^{-1}$). To monitor radiation damage, the concentrations, pH values and catalytic activities of the solutions were determined after the X-ray measurements. These concentration values were used to scale the X-ray data. The enzymatic activity was between 80 and 140% of its initial value, activities above 100% at higher pH values being possible in the presence of saturating concentrations of TDP and Mg^{++}.

X-ray solution scattering

The data were collected following standard procedures using the X33 camera (Koch and Bordas 1983; Boulin et al. 1986, 1988) of the EMBL on storage ring DORIS of the Deutsches Elektronen Synchrotron (DESY) and multiwire proportional chambers with delay line readout (Gabriel and Dauvergne 1982). Data were collected at two different camera lengths covering ranges of scattering vector $s = 4\pi \sin\theta/\lambda$ (2θ is the scattering angle and λ the wavelength) between $0.1 < s < 1.29\ nm^{-1}$ and $0.19 < s < 2.59\ nm^{-1}$. For the low angle measurements solutions with 3–5 mg/ml were used to avoid interparticle interference, whereas for the higher angles the concentrations were up to 10 mg/ml. The data were normalized to the intensity of the incident beam, corrected for the response of the detector, the scattering of the buffer was subtracted and the statistical errors were calculated using the program SAPOKO (Svergun and Koch unpublished). They were also scaled for concentration. Data from the two different s-ranges were merged by equalizing the average value of the scattering in the range $0.31 < s < 0.87\ nm^{-1}$. In this range of overlap, the effects of interparticle interference on the scattering curves of the most concentrated samples are negligible. Preliminary estimates of the particle sizes and of the information content of the data sets were obtained by a method based on orthogonal expansion (Svergun 1993). The experimental data were then processed using the program GNOMOKO, a version of the indirect transform program package GNOM (Svergun et al. 1988; Svergun 1991, 1992) running on IBM PC. The oligomer contents were calculated as described earlier (Koenig et al. 1992). The shapes of the dimers and tetramers were evaluated by multipole expansion (Stuhrmann 1970a, b; Svergun and Stuhrmann 1991). The three-dimensional density distribution $\varrho(r)$ of a homogeneous particle is represented in spherical coordinates (r, θ, φ) by an angular boundary function $F(\omega)$ of $\omega = (\theta, \varphi)$ such that $\varrho(r) = 1$ for $r < F(\omega)$ and $\varrho(r) = 0$ for $r > F(\omega)$. The boundary shape function is developed into a series of spherical harmonics $Y_{lm}(\theta, \varphi)$ as:

$$F(\omega) = b_0 \sum_{l=0}^{L} \sum_{m=-l}^{l} f_{lm}\, Y_{lm}(\omega)\,. \qquad (1)$$

Here the value of L determines the resolution (angular resolution is $\pi/(L+1)$). The coefficients f_{lm} are complex numbers with moduli not exceeding a value around 5 if one chooses the scale factor $b_0 \approx (3V/4\pi)^{1/3}$, where V is the particle volume. They are evaluated from the experimental intensities by a non-linear minimization procedure as described by Svergun and Stuhrmann (1991).

The scattering pattern of the tetramer and of the tetramer in the presence of pyruvamide (tetramer + PA) and the calculated shape of the dimers were used to determine the positions and relative orientations of the dimers in the tetramers following a general method described earlier (Svergun 1991). The method involves a non-linear minimization procedure yielding the translational and rotational parameters of the subunits given the scattering of the complex particle.

Results

The extended scattering curves of the solutions containing essentially dimers (pH 9.2) or tetramers (pH 6.5) are illustrated in Fig. 1. The orthogonal expansion method indicates that the scattering data from the dimer can be described by ten independent parameters and those of the tetramer and of the tetramer + PA by eleven independent parameters. The maximum sizes (D_{max}) of the dimer and native tetramer were found to be nearly identical, about 13 nm, whereas the size of the tetramer + PA is approximately 10% larger. These estimates of D_{max} were further confirmed by the indirect transform program GNOMOKO, which gave the best results using $D_{max} =$ 13 nm for the dimer and native tetramer and $D_{max} =$ 15 nm for the tetramer + PA. The processed scattering curves and the corresponding distance distribution functions are shown in Fig. 1 and the integral geometrical parameters of the different oligomers are summarized in Table 1.

Addition of DTE to the buffers resulted in a much higher stability of the samples in the X-ray beam as illus-

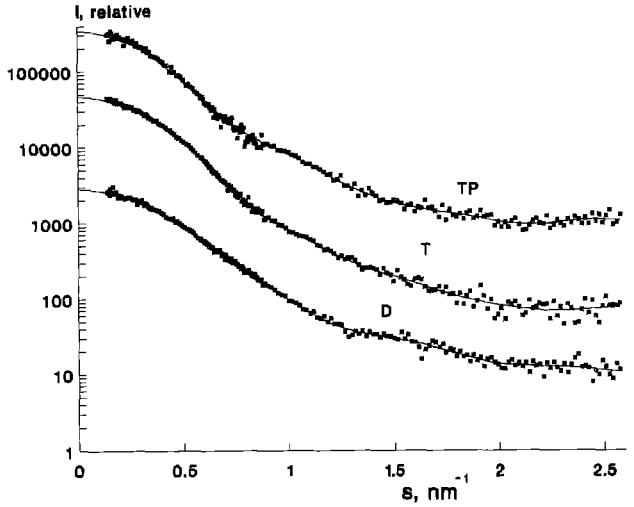

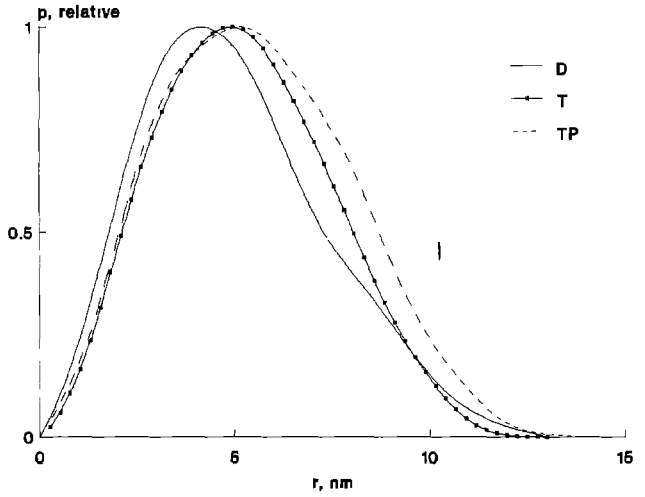

Fig. 1. *Left panel:* Scattering from dimers (D), tetramers (T) and tetramers with pyruvamide (TP): experimental data (*dots*) and fitted curves (*full lines*). The curves have been displaced by one logarithmic unit for better visualization. *Right panel:* Distance distribution functions $p(r)$ of the dimer (D), tetramer (T) and tetramer + PA (TP). The vertical bar indicates the largest propagated error

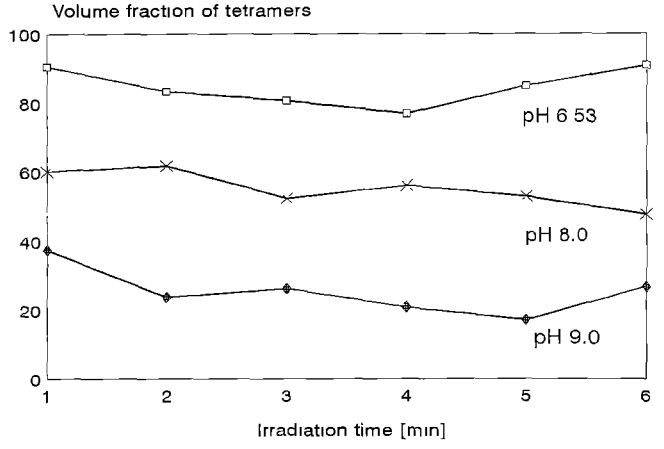

Fig. 2. Volume fractions of tetramers as a function of irradiation time for samples of pyruvate decarboxylase in buffers with different pH values containing 1 mM DTE

Table 1. Geometrical parameters of dimers and tetramers and their models

	R_g (nm)	Volume (nm^3)	D_{max} (nm)
Dimer			
Experimental	3.88 ± 0.04	210	13.0
Model	3.44	190	12.4
Tetramer			
Experimental	4.03 ± 0.03	381	13.0
Model	4.08	386	14.1
Tetramer + PA			
Experimental	4.30 ± 0.05	381	15.0
Model	4.28	380	14.7

trated in Fig. 2 and the scattering patterns at all pH values could be fitted satisfactorily as linear combinations of those of the dimers and tetramers only. This also confirms that the formation of octamers in the previous measurements (Koenig et al. 1992) was due to radiation damage.

The oligomer content as a function of pH for native PDC and in the presence of the non-competitive inhibitor phosphate, the activator pyruvamide (PA) and the cofactors thiamin diphosphate and Mg^{++} were calculated as described previously (Koenig et al. 1992) and the results are illustrated in Fig. 3. Native PDC in the range $5.5 < pH < 7.5$ is nearly completely tetrameric, between pH 7.5 and 9.5 there is an equilibrium between dimers and tetramers and above pH 9.5 the solutions contain nearly exclusively dimers. The effectors increase the tetramer fraction at higher pH-values and this effect is more pronounced with the cofactors, TDP and Mg^{++}. The volume fraction of tetramers is still 100% at pH 8.5 and even at pH 9.5 it still reaches 40%. The influence of phosphate and pyruvamide is less pronounced and although the onset of dissociation of the tetramers is not shifted to higher pH values, the volume fraction of the tetramers in the alkaline pH-range is higher than for native PDC. It reaches about 20% with pyruvamide and 25% with phosphate. Moreover, pyruvamide alters the conformation of the tetramers as indicated by the significant increase in radius of gyration (0.3 nm) and the discussion below.

The dimers and tetramers differ in sensitivity to radiation damage. Samples at high PDC concentration ($\cong$10 mg/ml) at pH 6.0 had 70–80% of their initial activity after irradiation whereas the samples at pH 9.0 only had about 20% remaining activity.

To determine the shape of dimers and tetramers in solution it is necessary to put the experimental data on an absolute scale (i.e. the forward scattering should be equal to the square of the volume of the particles in the homogeneous approximation). Some difficulties were encoun-

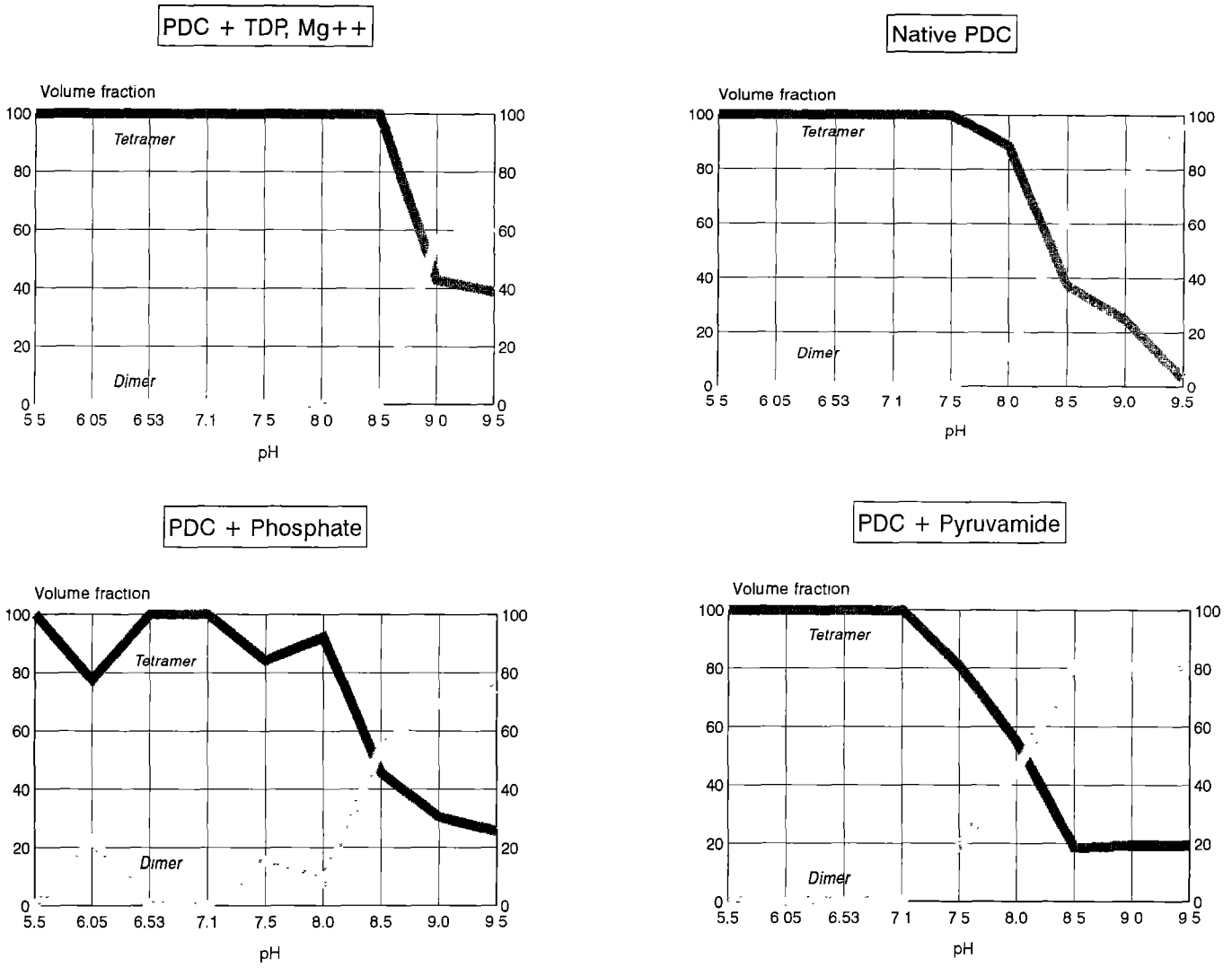

Fig. 3. Volume fractions of dimers and tetramers as a function of pH for native PDC and for PDC in the presence of various effectors as indicated

tered in determining the absolute scattering intensities of PDC solutions. In particular, using lysozyme solutions as the reference for absolute measurements yielded molecular weights of PDC that were somewhat (10–30%) lower than expected $4 \times 61\,000$ dalton (Hohmann and Cedeberg 1990). After elimination of the effects of radiation damage by addition of DTE and precise control of the pH dependent equilibrium it is still not straightforward to obtain accurate concentrations of PDC spectrophotometrically. The exact cause of this is not yet known but the extent of coenzyme binding may play a role. Concentrations measured independently on the same samples with 1:50 and 1:10 dilutions differed by 20–50%, the values at 1:10 dilutions being systematically higher.

For this reason the curves were scaled using the Porod volume, a parameter which does not depend on concentration. The Porod volumes given in Table 1 were evaluated from the outer parts of the scattering patterns following standard procedures (Feigin and Svergun 1987, p 80) and subtracting a constant to force a s^{-4} dependence on the intensities at larger angles. For subsequent calculations, the experimental curves for $0 < s < 2$ nm^{-1} renomalized to these volumes were used. Data for $s > 2$ nm^{-1}, where the contributions from inhomogeneities are significant, were discarded as they do not give additional information about the shape.

The shape of the dimer was first determined with a resolution of $L = 4$ in several independent runs starting from very different initial approximations (sphere, ellipsoid, various non-centrosymmetric particles). These calculations all led to similar elongated shapes with two domains characterized by negligible contributions from the odd harmonics, $l = 1$ and $l = 3$ and differing only by a rotation.

It is thus legitimate to omit these harmonics from the fit and to determine the shape of the dimer in the centrosymmetric approximation, thereby assuming that the two domains are identical at this resolution. The model with even harmonics up to $l = 4$ contains 13 parameters, the shape coefficients f_{lm}, three of which can be fixed to define the orientation of the particle. The restored shape of the dimer in the centrosymmetric approximation, shown in

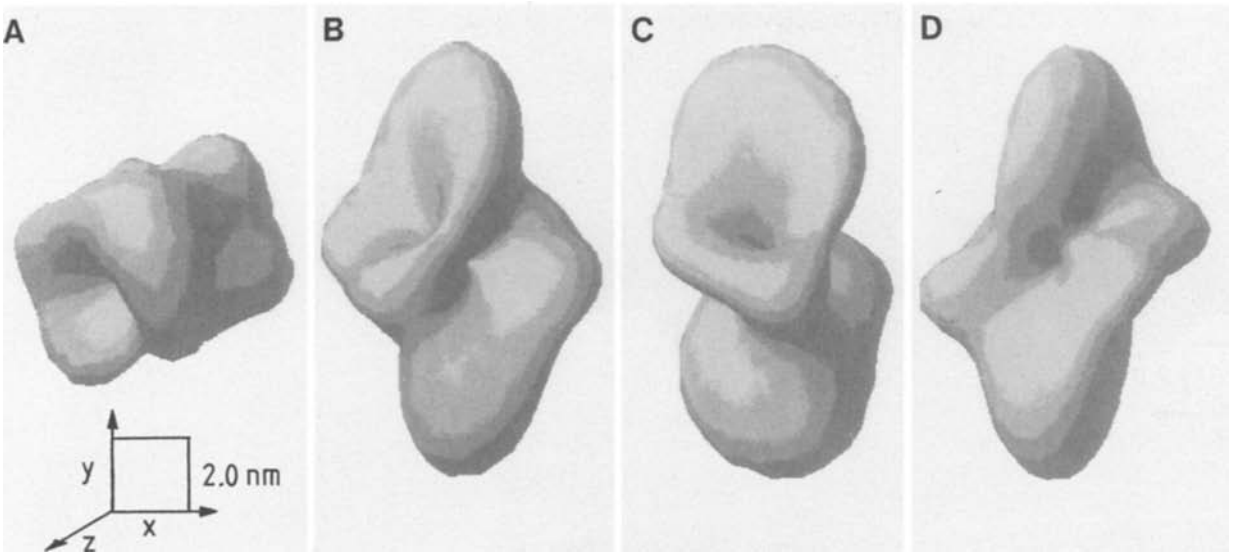

Fig. 4A–D. Shape of the dimer of PDC with a resolution of $L=4$. **A** View in the reference orientation looking down the z-axis. **B** Model **A** rotated by 90° around the x-axis. **C** Model **B** rotated 45° around the y-axis. **D** Model **B** rotated −45° around the y-axis

Table 2. Shape multipole coefficients of the models of the dimer and the tetramers

		Dimer		Tetramer		Tetramer + PA	
b0 (nm)		3.190		4.675		4.338	
l	m	Re	Im	Re	Im	Re	Im
0	0	3.345	–	3.197	–	3.291	–
2	0	0.862	–	0.433	–	0.618	–
2	1	0.154	−0.288	–	–	–	–
2	2	0.107	−0.139	0.300	–	0.413	–
3	2	–	–	–	0.166	–	0.221
4	0	0.532	–	−0.068	–	−0.055	–
4	1	−0.020	0.014	–	–	–	–
4	2	−0.311	0.420	0.220	–	0.231	–
4	3	−0.280	−0.406	–	–	–	–
4	4	0.129	0.253	0.159	–	0.174	–
5	2	–	–	–	0.095	–	0.052
5	4	–	–	–	0.151	–	0.291
6	0	–	–	0.135	–	0.071	–
6	2	–	–	0.030	–	0.105	–
6	4	–	–	0.181	–	0.236	–
6	6	–	–	0.033	–	−0.038	–

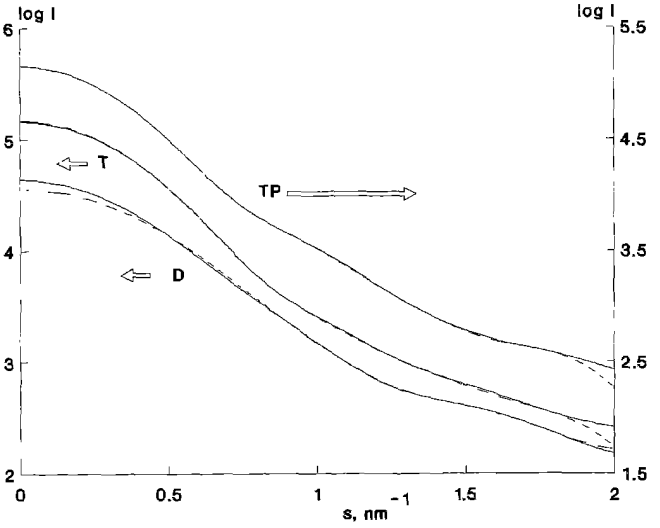

Fig. 5. Fit between the processed scattering curves (*full lines*) and the scattering from the models (*dashed lines*) of the dimer (D) in Fig. 4 and of the tetramer (T) and tetramer + PA (TP) in Fig. 6. The curves for TP is referred to the right ordinate axis which has been displaced by half a logarithmic unit for better visualization

Fig. 4, is thus described by ten independent parameters. The f_{lm} values corresponding to the reference orientation, shown in Fig. 4A, and later used to position the dimers in the tetramers, are given in Table 2. The residual R in terms of the experimental (I_{exp}) and calculated intensities (I_{mod})

$$R = \int_0^{s_{max}} |I_{exp}(s) - I_{mod}(s)|\, s^2\, ds \Big/ \int_0^{s_{max}} I_{exp}(s)\, s^2\, ds \qquad (2)$$

has a value of $R=3.9\%$ for the agreement illustrated in Fig. 5. Note, however, that, as indicated in Table 1, the geometrical parameters of the model are smaller than the experimental values. This results from the limited resolution cut-off of the series of spherical harmonics which, especially with anisometric particles such as the dimer, leads to lower R_g, V and D_{max} (Svergun and Stuhrmann 1991). As the limit of the homogeneous approximation has been reached, the resolution cannot be improved and the use of harmonics with $l>4$ would not be justified.

In the case of the tetramer, additional information can be used to achieve better resolution. Indeed, there are symmetry constraints on a stable tetramer formed by two dimers. The 222 symmetry which was previously found (Hübner et al. 1975; Müller et al. 1979) also exists in crystals of the α_4 homotetramer (Dyda et al. 1990). Since there are no significant differences between the α and β

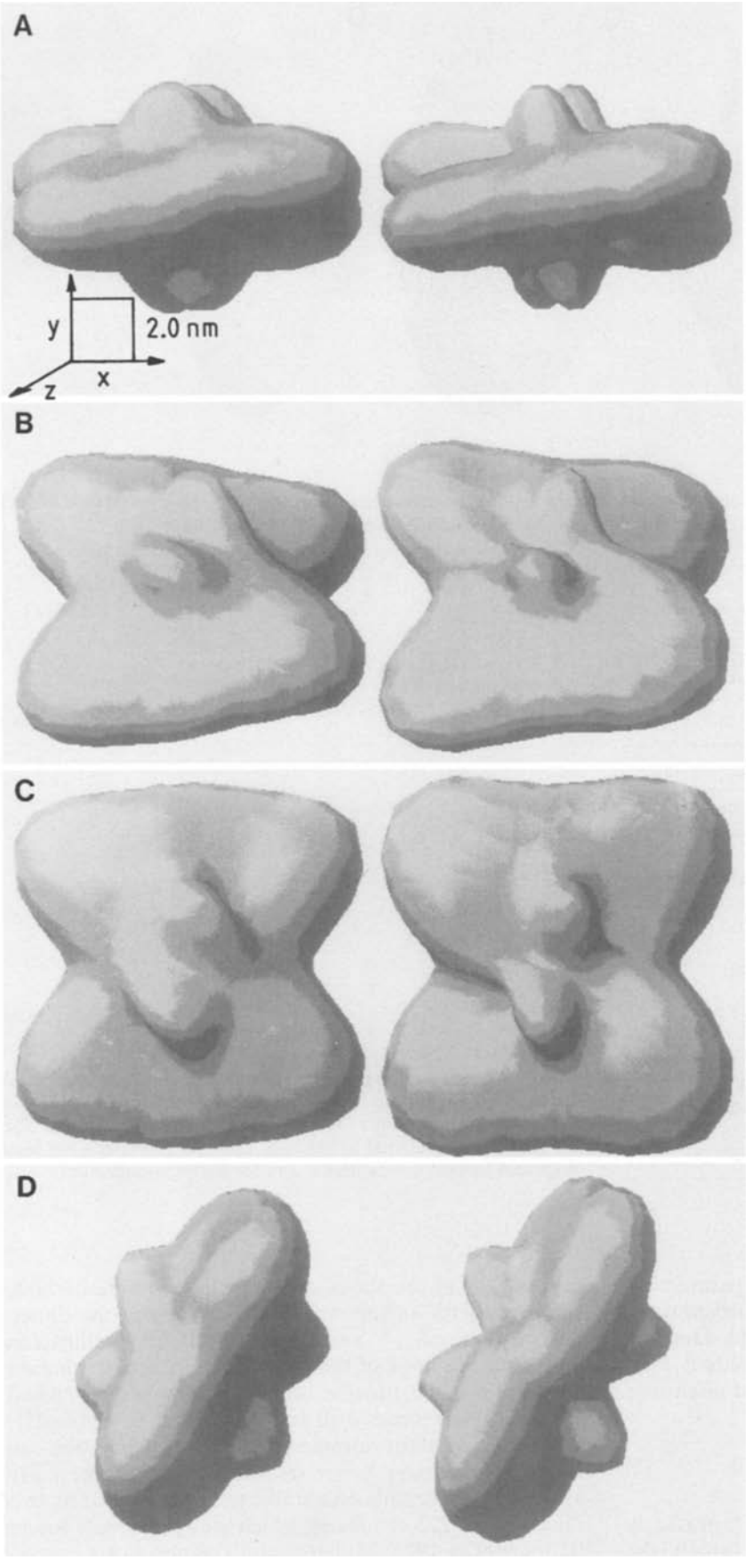

Fig. 6A–D. Shape of the native tetramer of PDC (*left*) and of the tetramer + PA (*right*) witl a resolution of $L = 6$. **A** view down the *z*-axis. The *x*-axis in this model corresponds approximately to the *z*-axis in the model of the dimer in Fig. 4. Models **A** rotated 45° **B** and 90° **C** around the *x*-axis. **D** Models in an orientation corresponding approximately to the reference orientation of the dimer

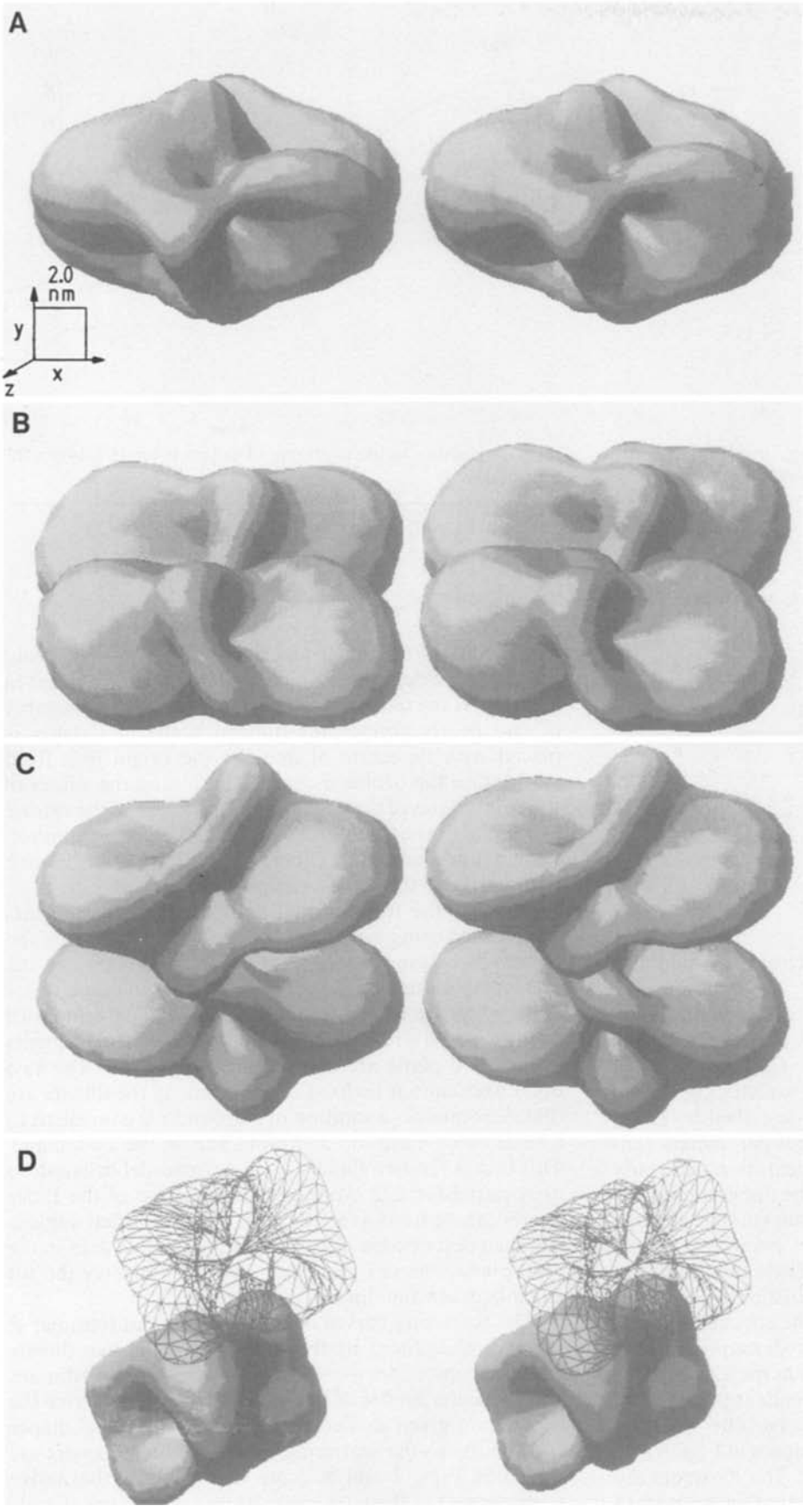

Fig. 7. Models of the native tetramer and of the tetramer + PA obtained by fitting the relative position of two dimers. The different views are chosen to correspond approximately to those in Fig. 6 The second dimer is shown as a wire frame in (D) for better visualization of the overlap

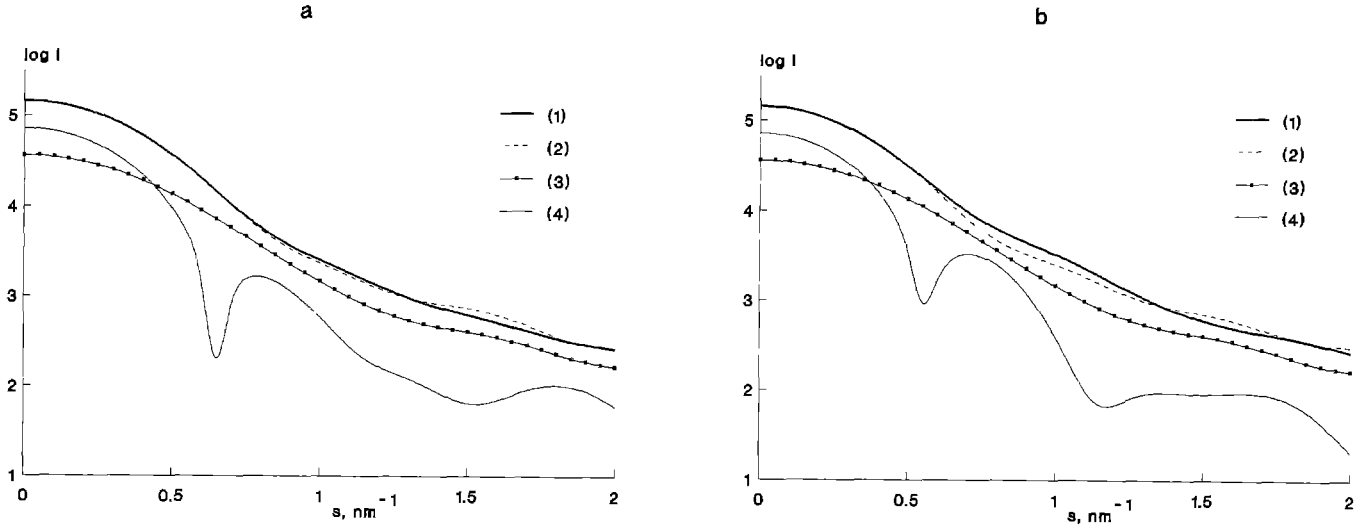

Fig. 8a, b. Best fit to the processed scattering curve (1) of the native tetramer (*left panel*) and of the tetramer + PA (*right panel*) of an assembly of two dimers (2). Scattering curve of an isolated dimer (3). Contribution to the scattering of the cross-terms between the two dimers (4)

Table 3. Positioning of the second dimer in tetramer and tetramer + PA

	Coordinates of the center of mass (nm)			Euler angles of rotation (deg)			Residual of the fit (%)
	x	y	z^a	α^a	β	γ^a	R
Tetramer	1.20	3.82	0	0	4.6	180	3.04
Tetramer + PA	0.99	4.69	0	0	8.6	180	9.40

[a] Parameter was fixed

subunits at low resolution the $\alpha_2\,\beta_2$ tetramer should also have 222 symmetry.

This imposes strong restrictions on the multipole coefficients and, if the symmetry axes coincide with the cartesian axes, all coefficients except f_{00}, f_{20}, Re $[f_{22}]$, Im $[f_{32}]$, f_{40}, Re $[f_{42}]$, Re $[f_{44}]$... vanish. The shape with a resolution up to $L=6$ is then described by 13 f_{lm} coefficients. The number of independent parameters cannot be reduced by rotation, as the orientation is already fixed. However, at higher resolution the integral parameters of the particle (i.e. radius of gyration, volume, average intraparticle distance) which are also invariants of the scattering curve, can be fitted neatly. These invariants are expressed as combinations of the f_{lm} coefficients (Svergun and Stuhrmann 1991) thus reducing the effective number of independent parameters. Hence, the description of the tetramer with a resolution up to $L=6$ in the 222 approximation involves again only ten independent parameters.

The shapes of the tetramer and the tetramer + PA restored in the 222 approximation are shown in Figs. 6 and 7 together with the corresponding fits. The R-factors are 1.4% and 0.9%, respectively. The structure parameters of the models are given in Table 1 and the f_{lm} coefficients for the orientation in Fig. 6A in Table 2.

Position of the dimers in the tetramer

The models of the dimer and the tetramer in Figs. 4 and 6 which were determined independently are consistent in as much as the tetramer can be described as the assembly of two nearly antiparallel dimers. If the first dimer is placed with its centre of mass at the origin in a fixed orientation the problem consists in finding the values of the coordinates of the centre of mass (r, θ, φ) of the second dimer and of the three Euler angles α, β, γ (for a definition see, e.g. Edmonds 1957, Chap. 1.3) describing the relative orientation of the second dimer.

Some of the translational and rotational parameters can be fixed using symmetry constraints by specifying the directions of the twofold axes in 222 symmetry. As the dimer is an elongated particle one axis, taken as the z-axis in the reference orientation in Fig. 4A, will coincide with its long axis. To retain 222 symmetry only displacements in the $z=0$ plane are allowed so that $\theta=\pi/2$. The two other axes cannot be fixed a priori but, as the dimers are centrosymmetric, a rotation of π around z is equivalent to a rotation of π around a twofold axis in the $z=0$ plane. This brings the two dimers in an antiparallel orientation as required for 222 symmetry. Hence, two of the Euler angles can be fixed as $\alpha=0$, $\gamma=\pi$. The azimuthal angle φ will then describe the directions of the twofold axes in the $z=0$ plane whereas the Euler angle β indicates the tilt angle between the dimers.

The scattering curves of the tetramer and tetramer + PA were thus fitted by the assembly of the two dimers with the constraints $\theta=\pi/2$, $\alpha=0$, $\gamma=\pi$. The coordinates and the Euler angles of the second dimer which give the best fit are given in Table 3. The corresponding shapes and the fits to the scattering curves of the tetramers are shown in Figs. 7 and 8. Note that both in the native tetramer and in the tetramer + PA the dimers are slightly tilted, e.g. the second dimer is rotated along the y axis, corresponding to the Euler angle β. The quality of the fit

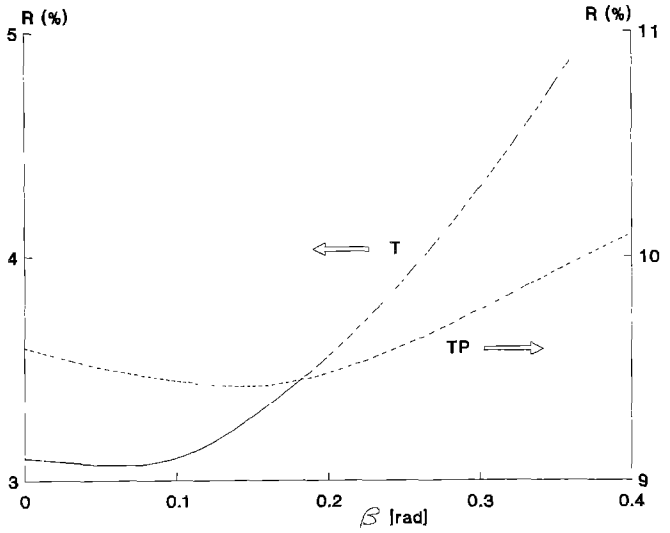

Fig. 9. Residual as a function of the tilt angle corresponding to the Euler angle β for the native tetramer (T) and for the tetramer with PA (TP). The latter refers to the right ordinate axis

depends significantly on this rotation, as illustrated in Fig. 9.

Discussion

The influence of the effectors correlates well with the kinetic observations. Phosphate stabilizes the tetramer as indicated by the shift of the dimer-tetramer equilibrium to higher pH values. These enhanced interaction in the tetramers can also explain that phosphate increases cooperativity while simultaneously reducing the affinity for the substrate (Boiteux and Hess 1970).

The significant conformational change of the tetramers induced by pyruvamide, which replaces the substrate as an activator, corresponds to the allosteric switch which results in the transition from a sigmoid rate curve to a hyperbolic one (Hübner and Schellenberger 1986).

The shape calculations for the dimer and the tetramer using the extended scattering data essentially confirm our previous results (König et al. 1992). The larger range of scattering vectors gives more reliable models especially for the shape of the dimers where two distinct domains, corresponding in all likelihood to the subunits, are clearly resolved. The dimensions are also in good agreement with those reported earlier (König et al. 1992). The structure is nearly centrosymmetric and the two subunits are thus identical at this resolution. This is in line with the fact that although PDC is usually described as an $\alpha_2 \beta_2$ tetramer, DEAE HPLC allows one to resolve six protein peaks and three distinct isoforms (α_4, β_4 and $\alpha_2 \beta_2$) (Farrenkopf et al. 1992).

The shapes of the native tetramers and of the tetramers + PA, although obtained completely independently, both display two distinct, slightly tilted, elongated subunits which can be unambiguously identified as dimers. The tilt angle between the dimers as measured from Fig. 6 is approximately 12° for the native tetramer and 20° for the tetramer + PA. When positioning the two dimers in the tetramers, the tilt angle is also larger for the tetramer + PA, $\beta = 9°$ compared to $\beta = 5°$ for the native tetramer. These tilt angles are smaller than those in Figs. 6 and 7. This is due to the zig-zag shape of the dimer illustrated in Fig. 4, which results in a tilt angle between monomers that is locally twice that between the dimers as can be seen in Fig. 7.

The scattering curve from the native tetramer can be well approximated by that of the assembly of two dimers in nearly antiparallel orientation, thus suggesting that only minor conformational changes take place upon formation of the tetramer. The tetramer + PA has a less compact structure, with a larger distance and larger tilt angle between the dimers. The fit using two dimers is also much poorer than for the native tetramer.

The number of independent parameters (ten) used to describe the models of the dimer and of the tetramers is formally justified from the point of view of information content. It is in agreement both with the results of the orthogonal expansion method (Svergun 1993) and with Shannon's theorem ($s_{max} \cdot D_{max}/\pi \approx 9$). Note that an additional parameter, the value of the forward scattering $I(0)$, is always added when the scattering curves are put on an absolute scale. We would like to stress, however, that the shapes should not be considered to be unique solutions. The interpretation of scattering data is always ambiguous, and different shapes could be found which produce practically identical scattering curves in the range of momentum transfer. The X-ray solution scattering curves are only approximations of the shape scattering curves, the latter could only be obtained by contrast variation. It is therefore not possible to use the data in the outer region ($s > 2$ nm^{-1}) to control the solution as the intensity in this range is biased by the scattering from the internal structure. With this caveat the models presented above can be considered to be reliable as they not only fit the scattering data and are consistent between each other, but also corroborate the results obtained by independent experimental techniques.

It will be interesting to compare the shapes calculated from the scattering curves and the relationship between the subunits with the forthcoming crystallographic structure of PDC (Dyda et al. 1990) bearing in mind, however, that the native conformation differs significantly from that of the active enzyme as indicated by the scattering experiments in the presence of pyruvamide.

References

Boiteux A, Hess B (1970) Allosteric properties of yeast pyruvate decarboxylase. FEBS Lett 9:293–296

Boulin C, Kempf R, Koch MHJ, McLaughlin SM (1986) Data appraisal, evaluation and display for synchrotron radiation experiments: hardware and software. Nucl Instrum Methods A249:399–407

Boulin CJ, Kempf R, Gabriel A, Koch MHJ (1988) Data acquisition systems for linear and area X-ray detectors using delay line readout. Nucl Instrum Methods A269:312–320

Dyda F, Furey W, Swaminathan S, Sax M, Farrenkopf B, Jordan F (1990) Preliminary crystallographic data for the thiamin diphos-

phate-dependent enzyme pyruvate decarboxylase from Brewer's yeast. J Biol Chem 265:17413–17415
Edmonds AR (1957) Angular momentum in quantum mechanics. Princeton University Press, Princeton
Farrenkopf BC, Bruce C, Jordan F (1992) Resolution of brewer's yeast pyruvate decarboxylase into multiple isoforms with similar subunit structure and activity using high-performance liquid chromatography. Prot Expr Purif 3:101–107
Feigin LA, Svergun DI (1987) Structure analysis by small angle X-ray and neutron scattering. New York, Plenum Press
Gabriel A, Dauvergne F (1982) The localisation method used at EMBL. Nucl Instrum Methods 201:223–224
Gish G, Smyth T, Kluger R (1988) Thiamin diphosphate catalysis. Mechanistic divergence as a probe of substrate activation of pyruvate decarboxylase. J Am Chem Soc 110:6230–6234
Hohmann S, Cedeberg H (1990) Autoregulation may control the expression of yeast pyruvate decarboxylase structural genes PDC1 and PDC5. Eur J Biochem 188:615–621
Holzer H, Schultz G, Villan-Palasi C, Jüntgen-Sell J (1956) Isolierung der Hefecarboxylase und Untersuchungen über die Aktivität des Enzyms in lebenden Zellen. Biochem Z 327:331–344
Hübner G, Schellenberger A (1986) Pyruvate decarboxylase – potentially inactive in the absence of the substrate. Biochem Int 13:767–772
Hübner G, Schellenberger A, Stelmaschuk VY, Kiselev NA (1975) Electron microscopic investigation of the subunit structure of yeast pyruvate decarboxylase. Acta Biol Med Ger 34:699–701
Hübner G, Weidhase R, Schellenberger A (1978) The mechanism of substrate activation of pyruvate decarboxylase. A first approach. Eur J Biochem 92:175–181
Koch MHJ, Bordas J (1983) X-ray diffraction and scattering on disordered systems using synchrotron radiation. Nucl Instrum Methods 208:461–469
König S, Svergun D, Koch MHJ, Hübner G, Schellenberger A (1992) A synchrotron radiation X-ray solution scattering study of the pH dependence of the quaternary structure of yeast pyruvate decarboxylase. Biochemistry 31:8726–8731
Müller JJ, Damaschun G, Hübner G (1979) Untersuchungen zur Struktur und Symmetrie der Pyruvat-Dekarboxylase aus Hefe mittels Röntgen-Kleinwinkelstreuung. Acta Biol Med Ger 38:1–10
Schellenberger A, Neef H, Golbik R, Hübner G, König S (1991) Mechanistic aspects of thiamine pyrophosphate enzymes via site-directed substitutions of the coenzyme structure. Biochem & Physiol of Thiamin Diphosphate Enzymes. VCH Weinheim: 3–15
Sieber M, König S, Hübner G, Schellenberger A (1983) A rapid procedure for the preparation of highly purified pyruvate decarboxylase from brewer's yeast. Biomed Biochim Acta 42:343–349
Stuhrmann HB (1970a) Interpretation of small-angle scattering functions of dilute solutions and gases. A representation of the structures related to a one-particle scattering function. Acta Crystallogr A26:297–306
Stuhrmann HB (1970b) Ein neues Verfahren zur Bestimmung der Oberflächenform und der inneren Struktur von gelösten globulären Proteinen aus Röntgenkleinwinkelmessungen. Zeitschrift für Physikalische Chemie Neue Folge 72:177–184
Svergun DI (1991) Mathematical methods in small-angle scattering. J Appl Crystallogr 24:485–492
Svergun DI (1992) Determination of the regularization parameter in indirect transform methods using perceptual criteria. J Appl Crystallogr 25:495–503
Svergun DI (1993) A direct indirect method of small-angle scattering data treatment. J Appl Crystallogr 26:258–267
Svergun DI, Stuhrmann HB (1991) New developments in direct shape determination from small-angle scattering. 1. Theory and model calculations. Acta Crystallogr A47:736–744
Svergun DI, Semenyuk AV, Feigin LA (1988) Small-angle scattering-data treatment by the regularization method. Acta Crystallogr A44:244–250
Zeng X, Chung A, Haran M, Jordan F (1991) Direct observation of the kinetic fate of thiamin diphosphate bound enamine intermediate on brewer's yeast pyruvate decarboxylase. Kinetic and regiospecific consequences of allosteric activation. J Am Chem Soc 113:5842–5849